

Palaeomagnetism and Geochronology of the Harrats Lunayyir and Khaybar Lava Fields, Saudi Arabia

Luigi Vigliotti, (Merry) Yue Cai, Najeeb M. A. Rasul, and Salem M. S. Al-Nomani

Abstract

To better constrain the tectonic history of the Arabian craton in the Tertiary, we carried out a combined paleomagnetic and $^{40}\text{Ar}/^{39}\text{Ar}$ geochronological study on volcanic rocks from the Khaybar and Lunayyir Harrats plus a site of sediments deposited below the Miocene rocks in the former area. Progressive thermal or alternating field demagnetization successfully isolated stable characteristic magnetizations (ChRM) that are consistent with a primary magnetization only in the Late Quaternary lava flows from Harrat Lunayyir. The Harrat Lunayyir paleomagnetic data set of 11 flow-mean directions ($D = 0.31^\circ$, $I = 36.9^\circ$, $\alpha_{95} = 10.5$) is statistically indistinguishable from the present field and the virtual geomagnetic poles (VGP: 214.1°E , 85.1°N ; $A_{95} = 12.3^\circ$) which indicate a negligible rotation ($R = -1.98 \pm 10.49^\circ$) with respect to the coeval African pole position. The paleomagnetic signal of the Miocene lava flows from the Harrat Khaybar area appear to be contaminated by the effect of lightning and weathering and consequently no tectonic/plate movement significance may be attributed to the large CCW rotation shown from 2 sites with antipodal directions. The direction of the high coercivity chemical remanent magnetization (CRM) isolated after thermal cleaning from the Pre-Miocene siltstones ($D = 169.6^\circ$, $I = -44.8^\circ$; $\alpha_{95} = 5.4^\circ$) is consistent with the few existing paleomagnetic results from Arabia. The associated VGP (314.4°E , 80.6°N) is close to the Pliocene VGP of the Arabian Plate and CCW rotated ($R = 14.86 \pm 6.38^\circ$) with respect to the Oligocene African VGP. The results imply

that the whole rotation of the Arabian Plate took place during the last phase (4–5 Ma) of the opening of the Red Sea, corresponding with the true sea floor spreading as already noted in the past by other authors. Whole rock $^{39}\text{Ar}/^{40}\text{Ar}$ step-heating analyses yield whole-rock plateau ages of 12.8 to 16.3 Ma for the alkaline lava flows from the Khaybar area, which is consistent with the estimated age range of the region-wide late Cenozoic alkaline volcanism in Saudi Arabia.

1 Introduction

The Red Sea has been considered the closest modern example of initiation of sea floor spreading between continental blocks (Wegener 1929; Bayer et al. 1989). The Red Sea was also one of the first oceanic basins to be interpreted in the context of plate tectonics theory (e.g., McKenzie et al. 1970) and to be included in a tectonic reconstruction based on paleomagnetic data (Irving and Tarling 1961). The Arabian Plate originated ~ 30 Ma by rifting of NE Africa to form the Gulf of Aden and the Red Sea. It contains extensive Cenozoic to Recent volcanic fields (harrats) dominated by alkali olivine basalts and hawaiite representing one of the largest alkali basalt provinces in the world (area $180,000 \text{ km}^2$). The Cenozoic basaltic lava fields of western Saudi Arabia were emplaced directly on the stable upper Proterozoic metavolcanics and granitic plutons of the Precambrian Arabian shield (Camp et al. 1991). The Arabian harrats are not associated with a well-developed continental rift system, such as the coeval lava fields of east Africa which are typical of the eastern margin of the Red Sea, but largely missing in the western margin on the African Plate. They occur on the uplifted eastern flank (rift shoulder) of the Red Sea depression in a tectonic environment similar to that of the continental basalt fields of eastern Australia (Johnson et al. 1989). In addition, their extension into Jordan, Syria, and Turkey, well beyond the northern latitude of the Red Sea

L. Vigliotti (✉)

Istituto di Scienze Marine, CNR Bologna, Bologna, Italy
e-mail: luigi.vigliotti@bo.ismar.cnr.it

(Merry)Y. Cai

Lamont Doherty Earth Observatory, Columbia University,
Palisades, NY, USA

N. M. A. Rasul · S. M. S. Al-Nomani

Center for Marine Geology, Saudi Geological Survey, Jeddah,
Saudi Arabia

suggests that they may be not strictly related to the rifting of Gulf of Aden/Red Sea (Camp et al. 1991).

Volcanic activity began during the Oligocene (30–31 Ma ago) with continental flood volcanism in northern Ethiopia, Eritrea and western Yemen which was coeval with the onset of rifting in the Gulf of Aden (Bosworth and Stockli 2016). Volcanism shifted from an initial tholeiitic and transitional composition to a more alkalic composition during the Miocene (<12 Ma ago) (Camp and Roobol 1992). It is generally agreed that the Oligocene alkali basalts around the Red Sea are associated with the divergence between the African and Arabian Plates (Brown 1970; Jones and Rex 1974; Coleman et al. 1977, 1979). However, it is unclear whether the rifting was passive or active and debates exist regarding the mechanism that drives the spreading and the development of the oceanic crust (e.g., Burke and Dewey 1973; Tapponnier and Francheteau 1978; Collins 2003). Stern and Johnson (this volume) propose that the Red Sea is a volcanic rifted margin (VRM) formed 20–24 Ma ago.

The exact timing of rifting and continental separation is unclear. Girdler and Styles (1974) suggested that an initial period of rifting and spreading occurred during late Eocene and Early Oligocene time (41–34 Ma ago) followed by a period of quiescence that ended as recently as 4–5 Ma, after which a new period of spreading began. Hall et al. (1976) and Hall (1979) pointed out that the onset of the initial spreading is not well-constrained by the interpretation of the magnetic anomalies, which can be indicative of two distinct periods either between 40 and 34 Ma or between 29 and 24 Ma. Cochran (1981) suggested that the rotation of Arabia away from Africa took place in late Oligocene to early Miocene with true seafloor spreading starting only about 4–5 Ma, when the Red Sea axial trough formed. McKenzie et al. (1970) calculated that about 7° of total rotation has taken place about a pole west of Greece (36°N, 17°E). Le Pichon and Francheteau (1978) suggested that this model only applies for the region of the Red Sea north of 18°N, while in the region south of 18°N the seafloor data indicate a spreading pole at 7°N, 50°E, south of the Red Sea, with about 3° of opening over the past 5 Ma about this pole.

Synthesizing available literature magnetic data, Hall (1979) suggested that the formation of the Red Sea can be best explained by 8.8° of counter-clockwise rotation of Arabia with respect to Africa associated with the early (main) period of opening, followed by 1.2° of rotation during the late (post 5 Ma) period of opening. He also suggested that the poles of rotation for the two periods are significantly displaced from each other (29°N, 27°E for early phase spreading and 45°N, 10°E for the later spreading), indicating that initially Arabia moved away from Africa more toward the north than the more recent E–W movement. The mean pole of rotation for an angle of opening of 9.9° is located at 31°N, 25°E. According to Roeser (1975), the axial

trough is underlain by oceanic crust and well-developed magnetic anomalies can be reconstructed back to anomaly 3 (about 5 Ma) from 16°N to 23°N, whereas Girdler (1983, 1985) suggests two or three phases for the opening of the Red Sea with an initial stage around 25 Ma ago and a third phase in the Plio-Pleistocene. The absence of magnetic anomalies older than Anomaly 3 hampers a detailed reconstruction of the plate motions before the Pliocene; however, Schettino et al. (this volume) suggests that the Euler poles of relative motions between the plates remained stable during most of the rifting stage.

Reilinger et al. (2015), based on GPS data, suggested that rifting in the Red Sea started at 22 ± 3 Ma, with an initial rate of extension across the rift at half of the present-day rate. At 11 ± 2 Ma, when rifting in the northern Red Sea shifted from the Gulf of Suez to the Red Sea/Aqaba fault system, the rate doubled to the current rate. On the base of geological data Bosworth and Stockli (2016) reach similar conclusions, dating the initial phase of extension at ~ 23 Ma.

The Arabian Plate was one of the first whose motion was investigated using paleomagnetic data (Irving and Tarling 1961). However, very few additional results have appeared in the literature since then. Kellogg and Reynolds (1983) published a few questionable data from Oligocene alkali basalts from As Sarat in the southern part of Arabia. Based on these data and new results from the younger Pliocene lava flows collected from Harrat Rahat, Hussain and Bakor (1989) defined a Tertiary apparent polar wander path (APWP) for Arabia characterized by the same clockwise loop detected in the African APWP during the Miocene to Holocene, with the best fit obtained by closing the Red Sea through a clockwise rotation of Arabia by an angle of 9° around the same pole indicated by Hall (1979) at 29.3°N, 27.1°E. An improvement in this fit included closing the Gulf of Aden through the shifting of the Arabian Plate by 120 km in a SSE direction, parallel to the Red Sea axial trough. The authors recognized that available data were few and far from satisfactorily accounting for the tectonics of the Red Sea. However, after more than a quarter of a century there are still no additional paleomagnetic data from this area that could better constrain the history of the Arabian Plate. The existing data are quite puzzling which make it difficult to constrain the timing of Red Sea opening and rotation. Thus, one of our goals was to estimate the extent of rotation of the Arabian plate since the beginning of the Red Sea opening and to constrain the timing of the rotation in recent times (late Quaternary).

In this work, we carried out a geochronological and palaeomagnetic study on 86 oriented hand samples collected from 20 sites that represent Cenozoic volcanic rocks from the lava fields in Harrats Lunayyir, Ishara, Al Kura and Khaybar located in the north-western region of Saudi Arabia in order to improve the resolution of the rotational history of

Arabia relative to Nubia during the past 30 Ma (Fig. 1). Previous attempts to determine the ages of Ishara, Al Kura and Khaybar rocks have been based on the K–Ar total fusion method with ages ranging from zero to 27 Ma (Camp and Roobol 1992). Duncan and Al-Amri (2013) conducted $^{40}\text{Ar}/^{39}\text{Ar}$ step-heating experiments on lavas from Lunayyir and found that most of the volcanism there occurred within the past 600 Ka. Here, we report new $^{40}\text{Ar}/^{39}\text{Ar}$ age determinations of Jabal Ishara, Jabal Anthar, Bi'r al' Ayn, Jabal Dhulay'ah and Jabal Jammazin on the same samples that have been used for paleomagnetic analysis.

2 Geological Framework and Sampling

We conducted field work in volcanic fields lying along the 25°N parallel, from the eastern Red Sea margin to ~150 km inland (Fig. 1a). Several recent lava flows perpendicular to the Red Sea margin dissect the Arabian coastal plain. Moving toward the east, one of the smaller and younger volcanic fields (Harrat Lunayyir) crops out, composed of relatively older flows in the south-western part and very young pyroclastic cones and flows that formed along related fissures. Some ~50 cinder cones form N–S and NW–SE trends and cover an area of about 3600 km² (Duncan and Al-Amri 2013) (Fig. 1b). The Lunayyir samples are generally fine-grained alkali olivine basalts and trachy-basalts with aphyric to only moderately phyric textures. Olivine and plagioclase phenocrysts are present within the groundmass that consists mainly of micro- to cryptocrystalline plagioclase and augite with minor olivine (Sanfilippo et al., this volume). To the east of Lunayyir, olivine basalts of Harrat Ishara occupy a highland area extending along the south-western margin of Wadi al Jiz'1 and Wadi Hamd (Fig. 1c). The volcanic field is deeply eroded with exposed basal units implying a relatively old age for the basalt preserved on the plateau relics. Along the eastern edge of the study area, to the east of Wadi al' Ays, basaltic lava flows form the most westerly part of the large Harrat Khaybar and of the smaller Harrat al Kura (Fig. 1c).

According to the geological maps (Kemp 1981) the collected rocks belong to Tertiary/Quaternary volcanic units (Tb; Qb) that characterize the Wadi al' Ays region, except for one site sampled at Jabal Bi'r al' Ayn that represents continental deposits that consist of red quartz-arenite and claystone of Eocene/Oligocene age underlying the volcanic units (Fig. 1d). These sediments offer the possibility of applying a tectonic correction to the paleomagnetic data that usually is impossible with volcanic rocks.

Hand samples were collected in the field and oriented using only a magnetic compass, which does not rule out the possibility of a bias in the magnetic direction due to large local magnetic anomalies from strongly magnetized rock

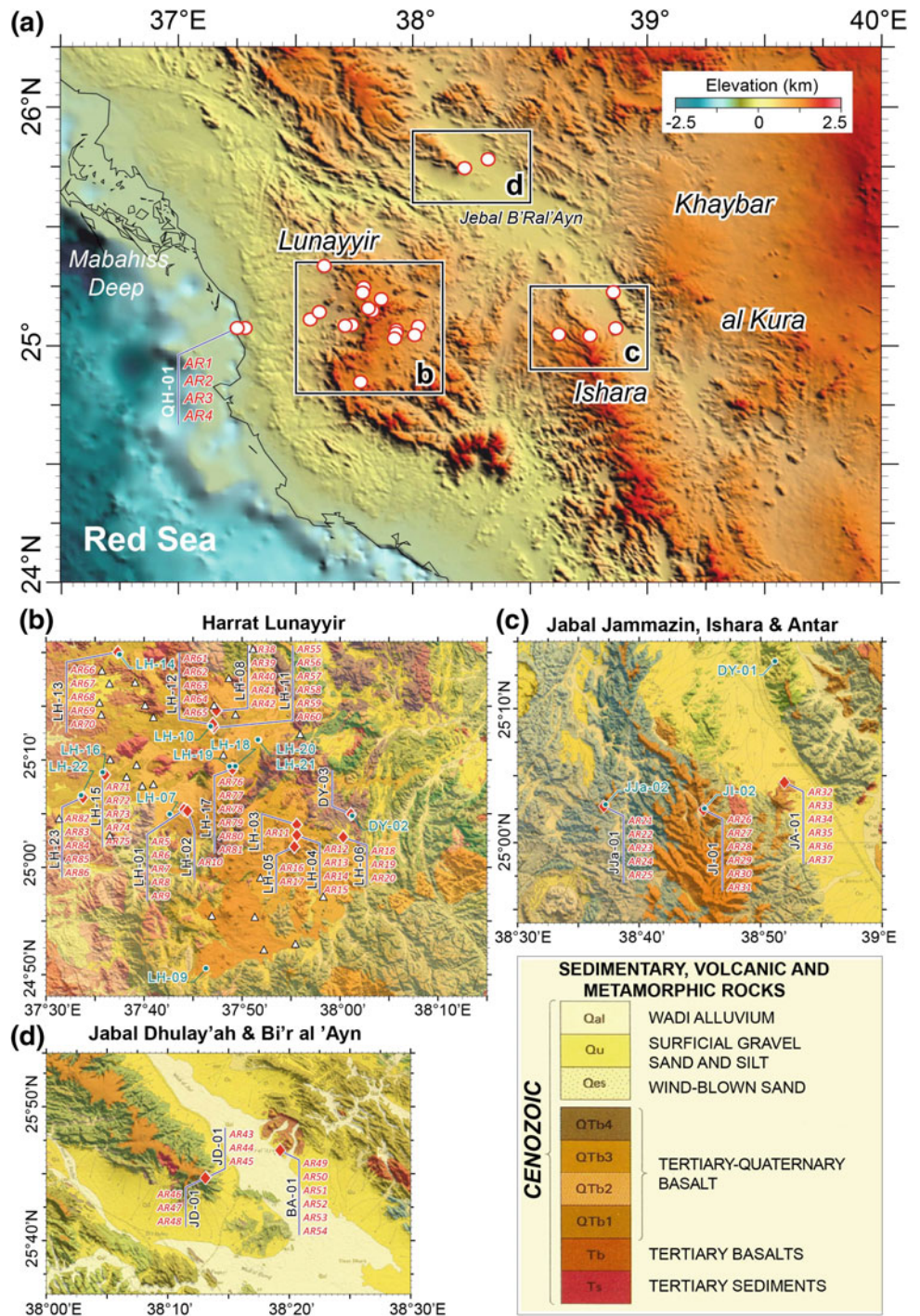
units. Deflection of the compass needle was observed in a few outcrops and a back-sighting technique was used to check the reliability of the orientation of the fiducial arrow marked on the rock. In a couple of outcrops, the local field was so strong that it was impossible to collect any oriented samples. Usually 4–6 hand samples were collected at each site, representing a typical paleomagnetic site, but at a few sites only 1–3 samples were included in the collection. It would have been desirable to get more samples from each lava flow, but the limited time for sampling and the roughness of the area hampered the possibility of improving on this number.

3 Methods

Between 1 and 5 standard paleomagnetic cylinders of 2.54 × 2.2 cm were drilled in the laboratory from each rock sample, for a total of 218 specimens. The natural remanent magnetization (NRM) was measured using a Molspin spinner magnetometer at the Paleomagnetic Laboratory of ISMAR-CNR at Bologna (Italy). Both alternating field (AF) (up to 80 mT) and thermal demagnetization (up to 600 °C) were carried out on pilot samples to check the reliability and the magnetic behaviour during the cleaning. Stepwise AF demagnetization was applied to the volcanics with an AGICO LDA-3A demagnetizer, while a MMTD1 furnace was used for thermal demagnetization of the sediments characterized by the presence of high coercivity minerals. The results were analysed by using the DAIE program (Sagnotti 2013) based on Fisher statistics (Fisher 1953) and principal component analysis (Kirshvink 1980). The mean directions were used to calculate the virtual geomagnetic pole (VGP) by using the PaleoMac program developed by Cogné (2003). Finally, the rotation with respect to Africa was evaluated following the procedure suggested by Demarest (1983) using coeval reference paleopoles from Torsvik et al. (2008). The site mean directions are given in Table 1. Magnetic susceptibility (κ) was measured for all but a few samples using a Bartington MS2 m. Hysteresis properties were measured at the INGV paleomagnetic laboratory in Rome by using a Micromag alternating gradient magnetometer (AGM-2900) with a maximum field of 1T. The ratio of the remanent magnetization to the induced magnetization produced by the Earth's field (29.86 A/m) was used to calculate the Koenigsberger ratio (Q). The results of these measurements are reported in Tables 2 and 3 for Khaybar and Lunayyir respectively.

$^{40}\text{Ar}/^{39}\text{Ar}$ age determinations were carried out at the AGES-laboratory at Lamont Doherty Earth Observatory of Columbia University using a Micromass VG 5400. The argon-isotopic ratios were determined in static mode using automated data collection software developed by Alan Deino

Fig. 1 Shaded relief map showing the major morphotectonic features of the northern Red Sea and adjacent volcanic lava fields on the western Arabian Plate with the locations of the sampling sites (**b**, **c**, **d**). Age assignments are based on morphologic data (relative extents of erosion, alteration, soil cover; Kemp 1981). Paleomagnetic samples are marked in red while blue colours indicate the samples used for ⁴⁰Ar/³⁹Ar age determinations. White triangles in Harrat Lunayyir refer to the samples studied by Duncan and Al-Amri (2013)



of the Berkeley Geochronology Center. Alteration of primary phases to secondary minerals is relatively limited in this very arid region. Thus, the volcanic samples were simply crushed and rinsed with deionized water. 0.5–1 mm representative rock chips without visible signs of alteration were selected under the microscope and co-irradiated with Fish Canyon sanidine at the USGS TRIGA reactor in Denver, CO, U.S.A for 8 h. The irradiated samples were placed

in Ta tubes, and evacuated in a chamber with a glass window for incremental heating with a diode laser (PhotonMachines). Stepwise heating of the samples was conducted with energies of 1–18 W, in increments designed to spread the ³⁹Ar out as much as possible. Released argon was cleaned of active gases by interaction with Zr-Al getters set at 2 amps, and then allowed into the Micromass VG5400 noble gas mass spectrometer for analyses using peak-hopping on an

Table 1 Paleomagnetic mean directions, Fisher statistics (K and α_{95}/A_{95} parameters) and Paleopoles for the studied sites. N/N_0 = number of samples used for the mean/number of measured samples. Qb, Tb in the age column refer to the stratigraphic age given in the geologic map (see Fig. 1)

Site	N/N_0	AGE		Decl (°)	Incl (°)	K	α_{95}/A_{95} (°)
QH-01	7/12	Qb		345.3	42.5	417.0	2.96
LH-01	9/11	Tb		352.2	34.0	170.0	3.96
LH-02	10/10	Qb		334.1	39.6	52.2	6.75
LH-04	10/11	Qb+Tb		353.2	40.5	108.1	4.70
LH-05	9/9	Tb		33.1	14.9	303.8	2.96
LH-06	6/7	Qb		344.8	19.9	23.5	14.10
LH-08	9/9	Tb		354.9	34.9	268.0	3.20
LH-11	12/12	Tb		14.7	40.3	72.5	5.10
LH-12	9/9	Qb		3.6	41.7	41.4	8.10
LH-15	12/12	Tb		355.6	51.8	130.5	3.80
LH-17	10/12	Qb		25.4	30.3	33.3	8.50
ALL	N = 11/11	Quaternary		0.31	36.9	19.8	10.5
			VGP	214.1 E	85.1 N	$P_{lat} = 20.6$	12.3
Selected	N = 9/11 (excl LH05-LH06)			358	40.4	36.6	8.6
		VGP	259.9 E	87.3 N	$P_{lat} = 23.1$	10.4	
BA-01	14/14	Oligocene?	Before TC	204.3	-38.2	3.5	24.8
BA-01	10/14		Selected	182.2	-30.7	43.7	7.4
BA-01	10/14		After TC	169.6	-44.8	82.3	5.40
				314.4 E	80.6 N	$P_{lat} = 26.4$	6.8
JJA-01	11/12	14.5±0.2		306.9	7.9	106	4.50
JD-01	9/9	13.2±0.6		343.0	64.0	163	4.00
JD-01	7/9	13.2±0.6		206.5	-18.1	627	2.40
JA-01	13/13	16.3±0.3		125.2	6.3	20.3	9.40
JI-01	12	14.6±1.7	Scattered	-	-	-	-

analogue multiplier. Argon data were corrected for backgrounds and discrimination using frequently measured blanks and air pipettes. Corrections were made for nuclear interferences using the information from Dalrymple et al. (1981) for the USGS reactor. The J-values were calculated from the average ages of Fish Canyon (FC) sanidines that were co-irradiated with the sample, for a given irradiation level assuming that the true age of FC is 28.201 ± 0.046 Ma (Kuiper et al. 2008).

4 Results

4.1 Ar/Ar Datings

Age determinations of samples selected from the top of the lava flow sequences and from the contact between volcanics

and the Precambrian basement at three major peaks of Harrat Ishara, now a deeply dissected plateau, range from 16.3 to 14.5 Ma (Table 4), in agreement with previously estimated ages ranging from 17 to 12 Ma (Bosworth and Stockli 2016). In particular, samples JJa-01/Tb-1 and JJa-02/Tb-2, representing the top and base of the ~500 m-thick volcanic sequence of Jabal Jammazin (Fig. 1c), after 9 and 7 heating steps, respectively, released plateau ages of 14.5 ± 0.2 Ma and 15.6 ± 0.8 Ma, respectively (Fig. 2). Although the two ages overlap within errors, they are consistent with their stratigraphic relationships. Sample JI-01/Tb-1 from the top of the ~300 m-thick sequence of Jabal Ishara (Fig. 1c), run in 8 heating steps, yielded a plateau age of 14.6 ± 1.7 Ma (Fig. 2c, d). The ~350 m-thick lava flow sequence of Jabal Antar (Fig. 1c) lies above a 50 m-thick sedimentary sequence resting above the Precambrian basement and includes boulder conglomerate and several upward-fining

Table 2 Natural remanent magnetization (NRM), magnetic susceptibility (κ) and Koenigsberger ratio (Q) of the volcanic rocks from the Khaybar area. NRM values in A/m, κ values in 10^{-5} SI units. Q was calculated by using a local magnetic field of 29.86 A/m

Samples	NRM	$\kappa(10^{-5}$ SI)	Q
AR-21aI	0.41	503	2.73
AR-22bII	0.64	487	4.41
AR-23aI	0.54	506	3.57
AR-24cII	0.41	559	2.48
AR-24bII	0.42	536	2.63
AR-25bI	0.53	657	2.72
AR-25dI	0.63	640	3.3
Site JJa-01 mean	0.51	555.43	3.12
AR-26bI	434	1288	1128.45
AR-26bII	349	996	1173.48
AR-27aII	73.2	977	250.92
AR-27b	72.7	895	272.03
AR-28	102	694	492.21
AR-29	478	613	2611.43
AR-30	25.9	790	109.8
AR-31aI	24.5	571	143.69
AR-31aII	16.4	458	119.92
AR-31b	26.6	486	183.3
Site JI-01 mean	180.57	833.73	672.89
AR-32a	0.3	486	2.05
AR-32bII	0.26	435	2.04
AR-33aI	0.3	428	2.35
AR-33aII	0.28	364	2.59
AR-33bI	0.32	385	2.77
AR-34bI	0.24	581	1.38
AR-34bII	0.25	536	1.54
AR-35	0.23	215	3.55
AR-36aI	0.16	250	2.21
AR-36aII	0.22	289	2.49
AR-36bII	0.2	257	2.65
AR-37a	10.7	454	78.93
AR-37c	11	477	77.23
Site JA-01 mean	1.88	396.69	13.98
AR-43a	1.77	610	9.72
AR-43b	1.75	597	9.82
AR-44aI	1.84	593	10.39
AR-44aII	1.92	605	10.63
AR-44cI	1.78	571	10.44
AR-44cII	1.85	612	10.12
AR-45a	102	672	508.32
AR-45b	70.5	615	383.91

(continued)

Table 2 (continued)

Samples	NRM	$\kappa(10^{-5}$ SI)	Q
Site JD-01A mean	22.93	609.38	119.17
AR-46aII	2.23	720	10.37
AR-46cI	1.99	725	9.19
AR-46cII	1.72	724	7.96
AR-47aI	4.71	761	20.73
AR-47bII	3.07	771	13.34
AR-47cI	3.9	690	18.93
AR-48aI	3.94	773	17.07
AR-48bII	2.81	773	12.17
AR-48bIII	3.59	740	16.25
Site JD-01B mean	3.11	741.89	14

sequences of coarse-grained sandstone to red siltstone with gypsiferous bases (Kemp 1981). Sample JA-01/Tb-1 from the base of this volcanic sequence, after 8 heating steps, yielded a plateau age of 16.3 ± 0.3 Ma (Fig. 2a, b), refining previously estimated ages of 20 Ma by Coleman et al. (1975) and 9 Ma by Dhellemmes and Delfour (1979).

Samples JD-01/Tb-1 and BA-01/Tb-1 from the northern sector of the study area are considered to be part of the Ishara volcanic field (Kemp 1981). Sample JD-01/Tb-1, recovered at the base of the volcanic sequence of Jabal Dhulay'ah (Fig. 1d), which is part of the Jabal Khirsat plateau, run in 9 heating steps, yielded a plateau age of 13.2 ± 0.6 Ma (Fig. 2g, h). Sample BA-01/Tb-1 (Fig. 1d) is from the top of a volcanic sequence that lies above a Cenozoic sedimentary sequence of poorly indurated argillo-arenaceous sediments (Pellaton and Dhellemmes 1978), and after 7 heating steps yielded a plateau age of 12.8 ± 0.13 Ma (Fig. 2e, f). This new age is younger than those estimated for the Ishara plateau basalts (~ 20 Ma, Coleman et al. 1975), which suggests that the Khirsat plateau basalts may be generated by a distinct volcanic event.

5 Paleomagnetism

5.1 Sediments

The sediments collected in the Bi'r al' Ayn (Site BA-01; Fig. 1d) region exhibit differences in the intensity of magnetization and magnetic coercivity reflecting changes in the magnetic mineralogy even in specimens drilled from the same hand-sample. Usually the NRM intensity is within 10^{-2} A/m, but significant variations up to one order of magnitude were observed even in specimens from the same

Table 3 Natural remanent magnetization (NRM), magnetic susceptibility (κ) and Koenigsberger ratio (Q) of the volcanic rocks from Harrat Lunayyir. NRM values in A/m, κ values in 10^{-5} SI units. Q was calculated by using a local magnetic field of 29.86 A/m

Samples	NRM	$\kappa(10^{-5}$ SI)	Q	Samples	NRM	K (10^{-5} SI)	Q	Samples	NRM	$\kappa(10^{-5}$ SI)	Q
AR-1a	1.57	488	10.77	AR-5aI	17	1284	44.34	AR-76aI	15.7	2590	20.3
AR-1b	1.58	501	10.56	AR-5bI	17.5	1368	42.84	AR-76bI	17.8	3315	17.98
AR-2aI	2.14	679	10.55	AR-6aI	7.79	2936	8.89	AR-77a	24.1	3032	26.62
AR-2aII	2.14	641	11.18	AR-6cII	7.41	2262	10.97	AR-77b	22.6	2956	25.6
AR-2bII	2.15	631	11.41	AR-7aII	2.76	1180	7.83	AR-78a	26.8	3789	23.69
AR-3aI	2.1	672	10.47	AR-7c	2.4	1095	7.34	AR-79a	13.6	3611	12.61
AR-3b	2.24	703	10.67	AR-8a	2.14	1580	4.54	AR-79b	7.73	4022	6.44
AR-4aI	1.68	541	10.4	AR-8b	1.96	1540	4.26	AR-80aI	21	6297	11.17
AR-4bII	1.71	542	10.57	AR-9aI	1.56	1240	4.21	AR-80aII	19.1	6159	10.39
AR-4aII	1.28	521	8.23	AR-9bII	2.15	1417	5.08	AR-81a	5.98	3755	5.33
AR-4c	1.34	540	8.31	AR-9cI	1.9	1349	4.72	AR-81b	6.03	3743	5.4
Site-QN mean	1.81	587.18	10.28	LH-0I mean	5.87	1568.27	13.18	LH-17 mean	16.4	3933.55	15.05
AR-55a	20.6	890	77.52	AR-71aI	4.55	1185	12.86	AR-66a	154	2500	206.3
AR-55b	19.5	655	99.7	AR-71bIII	4.26	1255	11.37	AR-66b	120	2405	167.1
AR-57a	6.63	3976	5.58	AR-72aI	7.68	602	42.72	AR-67aI	209	2075	337.32
AR-57b	6.09	3894	5.24	AR-73aI	4.09	1176	11.65	AR-67bI	233	2281	342.09
AR-57c	7.42	4167	5.96	AR-73bII	6.16	757	27.25	AR-68aII	268	1951	460.03
AR-58a	7.84	2488	10.55	AR-73aII	5.35	912	19.65	AR-68bI	185	1975	313.7
AR-58bII	7.91	2401	11.03	AR-73bI	5.32	897	19.86	AR-69aII	6.5	493	44.15
AR-58c	7.26	2296	10.59	AR-74bII	8.96	695	43.18	AR-69bI	6.16	463	44.56
AR-59a	7.09	3150	7.54	AR-74c	8.14	625	43.62	AR-69c	6.65	453	49.16
AR-59b	6.99	2701	8.67	AR-75aII	5.77	796	24.28	AR-70aII	24	518	155.16
AR-60b	12.6	4594	9.19	AR-75bI	6.99	898	26.07	AR-70bI	25.3	750	112.97
LH-11 mean	9.99	2837.45	22.87	LH-15 mean	6.12	890.73	25.68	LH-13 mean	112.51	1442.18	202.96
AR-38aI	26.5	6410	13.85	AR-11aII	2.46	1047	7.87	AR-61aII	6.31	4447	4.75
AR-38bII	23.7	7066	11.23	AR-11bI	9.34	1914	16.34	AR-61aIII	8.64	4281	6.76
AR-39aI	11.9	5499	7.25	AR-12a	1.83	405	15.13	AR-62aII	9.88	4008	8.26
AR-39bII	10.2	5317	6.42	AR-12b	2.23	523	14.28	AR-62b	7.11	4592	5.19
AR-40aII	9.32	6000	5.2	AR-13bI	2	433	15.47	AR-63aI	18.5	5321	11.64
AR-40bI	9.02	4917	6.14	AR-14aI	2.87	1117	8.6	AR-63bI	30.6	4879	21
AR40cII	10.3	4902	7.04	AR-14b	3.1	1137	9.13	AR-64a	47.2	4774	33.11

(continued)

Table 3 (continued)

Samples	NRM	$\kappa(10^{-5} \text{ SI})$	Q	Samples	NRM	K (10^{-5} SI)	Q	Samples	NRM	$\kappa(10^{-5} \text{ SI})$	Q
AR-42a	10.6	5193	6.84	AR-15aI	3.13	331	31.67	AR-64b	32.5	5113	21.29
AR-42c	13.9	5121	9.09	AR-15aII	3.37	354	31.88	AR-65BI	34.5	5891	19.61
LH-08 mean	13.94	5602.78	8.12	LH03-04 mean	3.37	806.78	16.71	LH-12 mean	21.69	4811.78	14.62
AR-82bI	12.2	2558	15.97	AR-16aIII	3.87	1882	6.89	AR-18a	39.6	2065	64.22
AR-83aI	6.29	862	24.44	AR-16bI	3.73	1997	6.26	AR-18bI	32.7	1851	59.16
AR-83b	6.21	845	24.61	AR-16bII	4.43	1882	7.88	AR-18bII	32.5	2451	44.41
AR-84aII	9.17	3116	9.86	AR-16cI	3.73	1600	7.81	AR-19b	37.9	3605	35.21
AR-84bI	3.37	3213	3.51	AR-17aII	4.15	1119	12.42	AR-19c	40.9	3709	36.93
AR-84cI	6.53	2947	7.42	AR-17aIII	3.97	1355	9.81				
AR-85aI	9.9	2764	12	AR-17bI	3.62	1220	9.94				
AR-85aIII	5.18	1194	14.53	AR-17bII	5.15	1737	9.93				
AR-86aI	18.3	4067	15.07	AR-17cI	4.61	1300	11.88				
AR-86aII	16.3	4140	13.19								
LH-23 mean	9.34	2570.6	14.06	LH-05	4.14	1565.78	9.2	LH-06 mean	36.72	2736.2	47.99

Table 4 $^{40}\text{Ar}/^{39}\text{Ar}$ ages of the volcanics from the Khaybar area. Three types of ages are reported with the preferred ages shown in bold: (1) integrated ages are obtained by summing all of the argon fractions extracted during a step-heating experiment; (2) isochron ages are calculated from regression analysis of $^{36}\text{Ar}/^{40}\text{Ar}$ vs. $^{39}\text{Ar}/^{40}\text{Ar}$ data; (3) plateau ages are calculated based on trapped initial $^{36}\text{Ar}/^{40}\text{Ar}$ values calculated from the isochrons and are defined as the weighted mean age of three or more contiguous heating steps that correspond to a minimum of 50% of the ^{39}Ar released. Column N lists the number of heating steps used to calculate the plateau/the total number of heating steps

$^{40}\text{Ar}/^{39}\text{Ar}$ age determination

Sample	Integrated age (Ma)	2σ error (Ma)	Plateau age (Ma)	2σ error (Ma)	N	MSWD	Isochron age (Ma)	2σ error (Ma)	$^{40}\text{Ar}/^{36}\text{Ar}$ initial	2σ error
JA01-TB-1	16.3	1.3	16.3	0.3	7/7	0.4	16.3	0.4	301	3
JJ01/Tb-1	14	2	14.6	1.7	6/8	0.09	14.7	1.8	293	10
BA01/Tb-1	25.9	1.4	12.8	0.13	6/9	0.33	12.8	0.2	304	2
JD01/Tb-1	13.1	1.6	13.2	0.6	6/9	0.03	13.2	0.8	297	7
JJa-01/Tb-1	14.3	0.4	14.5	0.2	8/9	0.13	14.5	0.3	299	4
JJa02/Tb-2	15	3	15.6	0.8	4/7	0.24	15.5	1.2	301	3

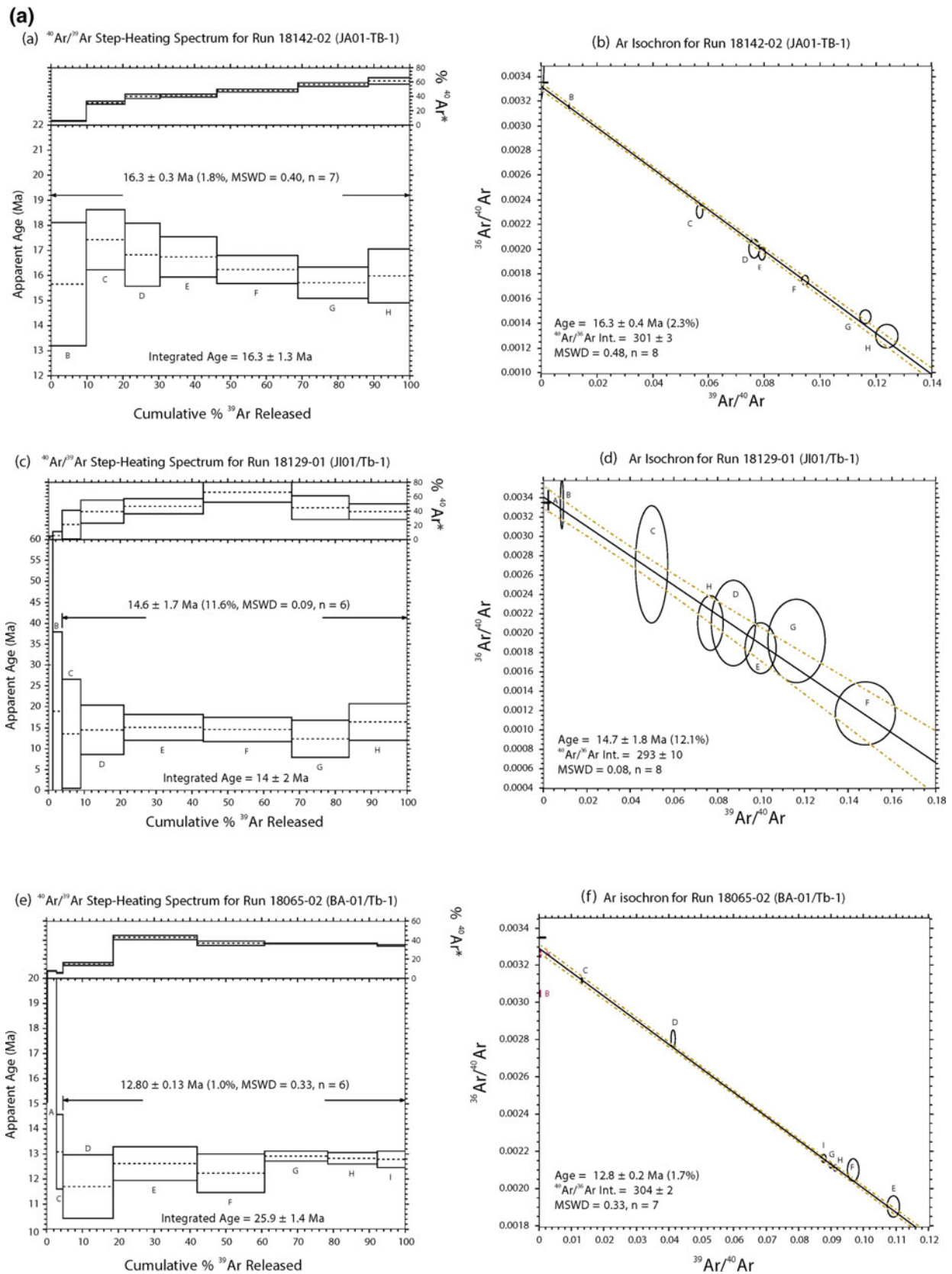


Fig. 2 Radiometric dating of the studied samples (2a and 2b). Step-heating spectra (diagrams a-c-e) and isochrons (diagrams b-d-f) of the whole-rock $^{40}\text{Ar}/^{39}\text{Ar}$ analyses. The apparent ages reported on the step-heating spectra are calculated using trapped initial Ar compositions that are delineated by the isochron of the same sample. The associated raw data are reported in Table 2. 1SD errors are shown as boxes and

ellipses about the mean values. The first two heating steps of BA-01/Tb-01 in panels e and f show anomalously old ages at very low percent radiogenic $^{40}\text{Ar}^*$. These steps likely reflect secondary effects and are therefore excluded from the calculations for the plateau and isochron ages

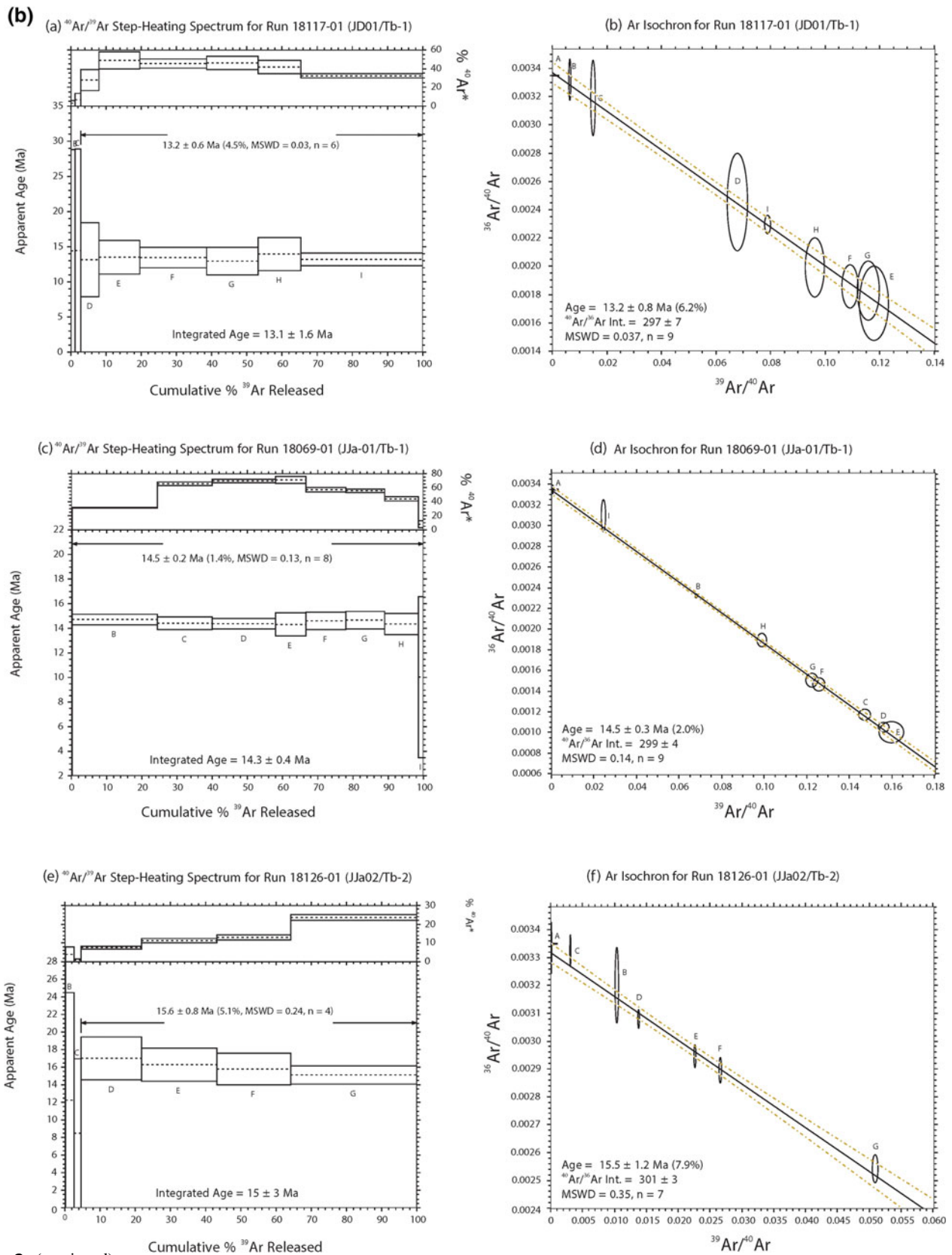


Fig. 2 (continued)

sample. The stepwise thermal demagnetization (Fig. 3a) result shows that a significant amount of magnetization survives at temperatures of 570–600° C (i.e., AR-54bIII, AR-49aII; Fig. 3b, c), which suggests that hematite is the carrier of the remanence as also indicated by the reddish colour of the rock. However, some samples lost part of their magnetization at lower temperatures (i.e., AR-49aII; Fig. 3a, c) and even AF treatment (AR-52bI; Fig. 3d) appears able to remove part of the magnetization, indicating that the hematite content is not constant. This is confirmed by the differences in the hysteresis properties, with coercivity of the remanence (B_{cr}) ranging from 32.4 mT in sample AR-51 (Fig. 3e) to 158.9 mT in sample AR-52 (Fig. 3f). The differences in the magnetic mineralogy appear to play a role in the paleomagnetic record, with stable and clear paleomagnetic directions isolated only from samples characterized by hard coercivity. All the samples exhibit negative inclinations, which indicate that the present field is not responsible for the observed directions. After the tectonic corrections, 10 out of 14 specimens give means of $D = 169.6^\circ$, $I = -44.8^\circ$ with an $\alpha_{95} = 5.4^\circ$ (Fig. 4). The interpretation of the paleomagnetic data should take into account that the sampling was restricted to a small outcrop and the results confined to the samples collected from a thin layer that possibly represents a post-depositional chemical remanent magnetization (CRM). It cannot be excluded that this CRM could have been acquired during a time interval that was insufficient to fully average the secular variations. The grouping of the paleomagnetic directions appears to become better after the tectonic correction (Fig. 4) which indicates that the age of the magnetization predates the tilting of the rock. The associated VGP is Long: 316.2°E, Lat: 80.6°N, $K = 4.3^\circ$, $A95 = 6.8^\circ$, $Plat = 26.4^\circ$ N.

5.2 Miocene Lava Flows

Scattered results mostly with shallow and negative inclinations characterize the paleomagnetic directions measured in the lava flows of Miocene age. The magnetic content of the rock appears very variable between and even within each site, with differences well represented by magnetic behaviour during thermal (Fig. 5a) and AF demagnetization (Fig. 5b). Almost certainly, weathering plays an important role in the magnetization of these rocks. Most of the rocks exhibit a secondary overprint, probably of viscous origin. This secondary overprint is removed after AF cleaning at 5–10 mT, after which the directions stabilize indicating the presence of a stable vector representing the Characteristic Remanent Magnetization (ChRM) (Fig. 5c). As shown in the plot of the induced magnetization (J_i) versus NRM (Fig. 6), the lavas from Jabal Jammazin (JJa-01) and Jabal Anthar (JA-01) yield a quite weak NRM intensity ($J < 1$

A/m) with low Koenigsberger ratio ($Q < 5$) whereas scattered and very high NRM values (up to 10^2 A/m), with low coercivity (median destructive field, MDF < 5 mT) and high Koenigsberger ratio ($Q > 100$), occur in the rocks collected at Jabal Ishara (JI-01) (Table 2). Probably lightning strikes are responsible for the magnetization measured at this site, and the scattered directions (Fig. 7) should be considered unreliable for any paleomagnetic discussion. More constant values of both NRM and J_i characterize the lavas in the northern area of Jabal Dhulay'ah (JD-01) (Fig. 6), with two close lava flows showing a different polarity (Fig. 7) with a normal/reverse (N/R) stratigraphic sequence. If no significant time gap occurred between the two flows the Ar/Ar dating of the rock (13.2 ± 0.6 Ma) indicates that they can be correlated with one of the few N/R sequences occurring within the chron C5A (5AB-5AA) that characterizes the first half of the Serravalian (Gradstein et al. 2012). The mean values exhibit conflicting directions in terms of both declination and inclination ($D = 343^\circ$, $I = 64^\circ$, $\alpha_{95} = 4^\circ$; $D = 206.5^\circ$, $I = 18.1^\circ$, $\alpha_{95} = 2.4^\circ$) (Fig. 7; Table 1), but are still in the range of the secular variation. Antipodal directions characterize the paleomagnetic directions measured in the rocks from Jabal Jammazin (JJa-01, $D = 306.9^\circ$, $I = 7.9^\circ$) and Jabal Anthar (JA-01, $D = 125.1^\circ$, $I = 6.3^\circ$) (Fig. 7; Table 1), with shallow inclinations that, coupled with the already discussed weak intensity of magnetization, make suspicious the source of the magnetization. The scatter of the results does not allow the calculation of a mean value that can yield a VGP representative of the Miocene direction for the Arabian Plate.

5.3 Quaternary Lava Flows

The lava flows collected from Harrat Lunayyir display a stable behaviour with only a minor viscous secondary overprint, which could be removed in the early steps (< 10 mT) of AF demagnetization (Fig. 8) that were applied to these volcanics as a cleaning procedure. Most of the magnetization shows a spectrum of coercivity restricted within 20–25 mT (Fig. 8) with a MDF < 10 mT reflecting a predominance of MD grain size. The plot of J_i versus NRM shown in Fig. 6 attests to a better grouping of the Lunayyir samples with respect to the Miocene volcanics. The Q ratio is mainly between 5 and 70, with higher values only measured in a few samples from site LH-13 likely affected by lightning (Table 3, Fig. 6). After cleaning, the paleomagnetic directions show a normal polarity except for the above-mentioned samples from site LH-13 (Fig. 9). The results of this site have not been included in the calculations of the Fisher's statistics. A poor grouping characterized also Site LH-06 ($\alpha_{95} = 19.9^\circ$) and a few samples from other sites (i.e., LH-17) that lie far from the mean, although they did not

Fig. 3 Normalized intensity of magnetization (a), orthogonal vector diagrams (tilt corrected) during thermal (b, c) and AF (d) cleaning and hysteresis loops (e, f) for representative samples of pre-Miocene sediments. Red (blue) circles represent projection onto the horizontal (vertical) plane

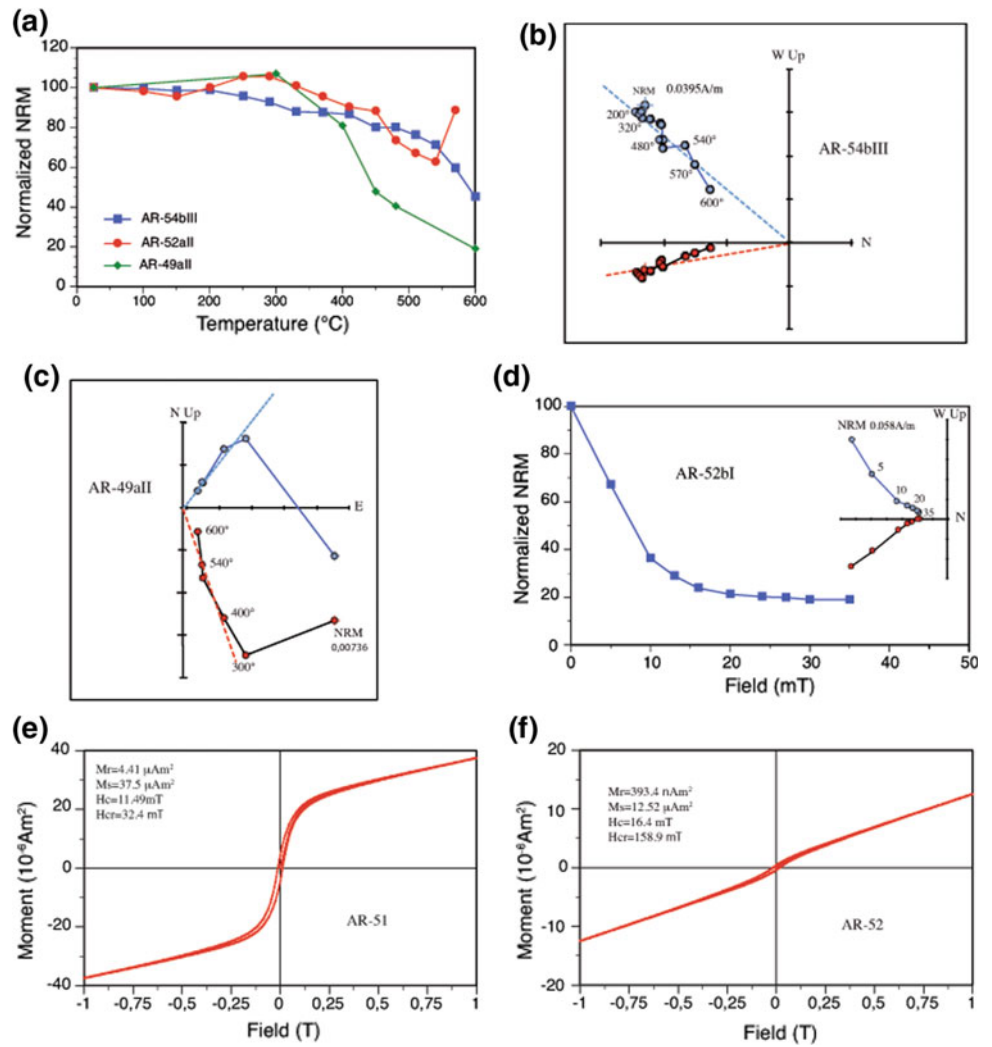


Fig. 4 Equal area projection of the paleomagnetic data from the pre-Miocene sediments collected at Bi'r al 'Ayn before and after tectonic correction. Open (closed) symbols refer to negative (positive) inclinations. Open circles in blue represent the MAD of each sample and the α_{95} for the mean values (red square)

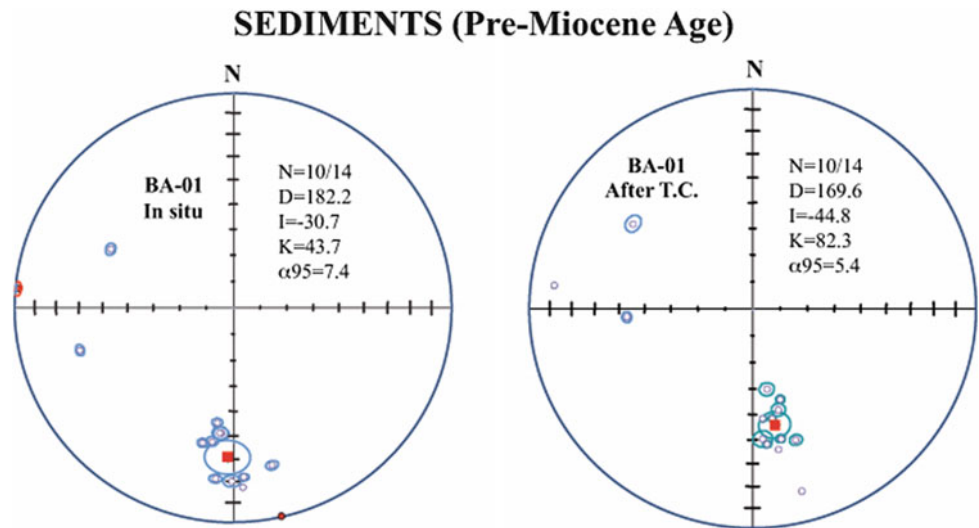


Fig. 5 Normalized intensity of magnetization during thermal (a) and AF (b) cleaning, and orthogonal vector diagrams (c) for representative samples of volcanic lava flows of Miocene age. Red (blue) circles represent projection onto the horizontal (vertical) plane

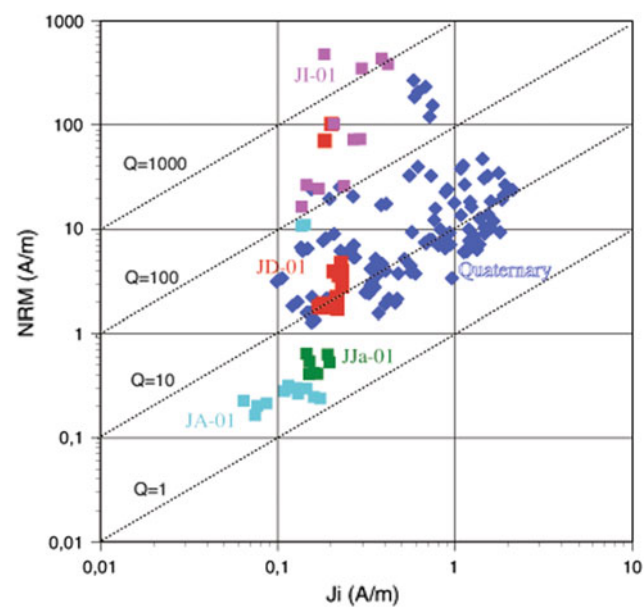
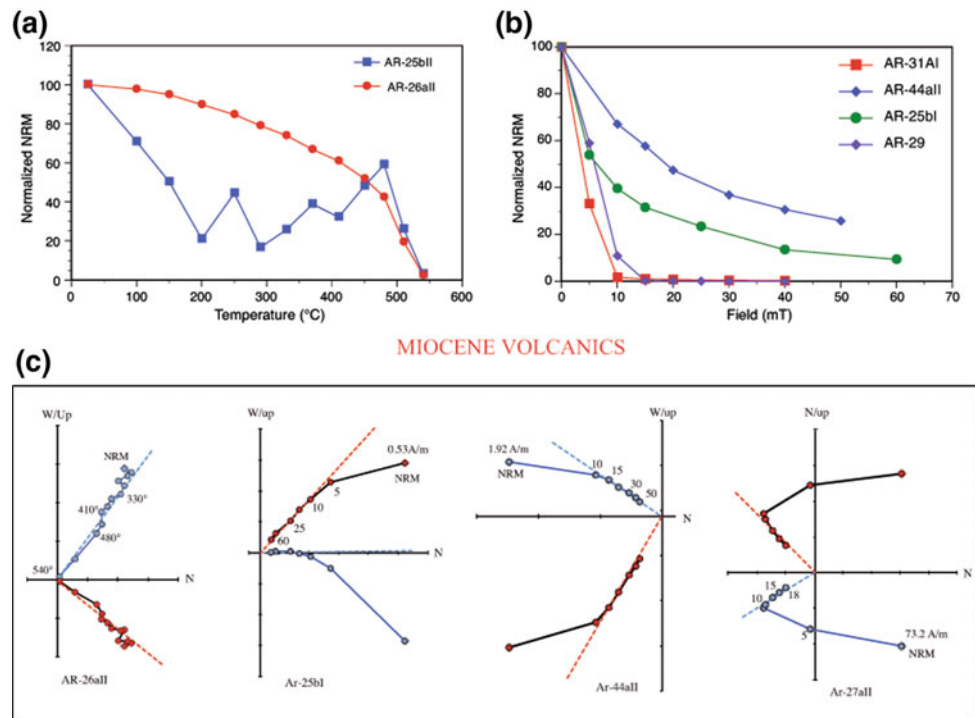


Fig. 6 Induced magnetization (J_i) versus NRM for the Miocene volcanics from Harrat Khaybar (Sites JA-01; JJa-01; JD-01; Ji-01) and the Quaternary lavas from Lunayyir

exhibit directional change during AF demagnetization. The nature of the outcrops restricted the sampling to the surface of the lava flows so it is possible that these samples may have been displaced during the acquisition of their thermoremanent magnetization (TRM). They have been excluded in the calculations of the means.

The results from the 11 sites with reliable magnetization measurements clustered around a mean value of $D = 0.31^\circ$, $I = 36.9^\circ$ with statistical parameters $K = 19.8$ and $\alpha_{95} = 10.5^\circ$ (Fig. 10; Table 1). An improvement of the clustering ($D = 358^\circ$, $I = 40.4^\circ$; $K = 36.6$; $\alpha_{95} = 8.6^\circ$) with an inclination that is closer to the expected value for the latitude of the sites (43°) can be obtained by excluding the mean values of sites LH05 and LH06 with shallower inclinations (Table 1). However, considering that the results are restricted to 11 sites we prefer to use the whole data set for a better average of the secular variation. The mean direction for the Lunayyir volcanics corresponds to a pole position at 85.1° N Lat., 214.1° E Long (Fig. 11; Table 1).

6 Discussion and Conclusions

As discussed previously the ChRM of the rocks was isolated from most of the studied sites, but only for the Quaternary volcanics can it for certain be considered representative of a primary magnetization. The CRM carried by the high coercivity minerals present in the red siltstone from the Bi'r al' Ayn region could be younger than the Oligocene age of the rock but the reverse polarity indicates that it is certainly older than the Brunhes (0.78 Ma). The mean declination value (169.6°) is compatible with the counter-clockwise rotation of the Arabian Plate established by the existing paleomagnetic results. Nevertheless, the inclination (44.8°)

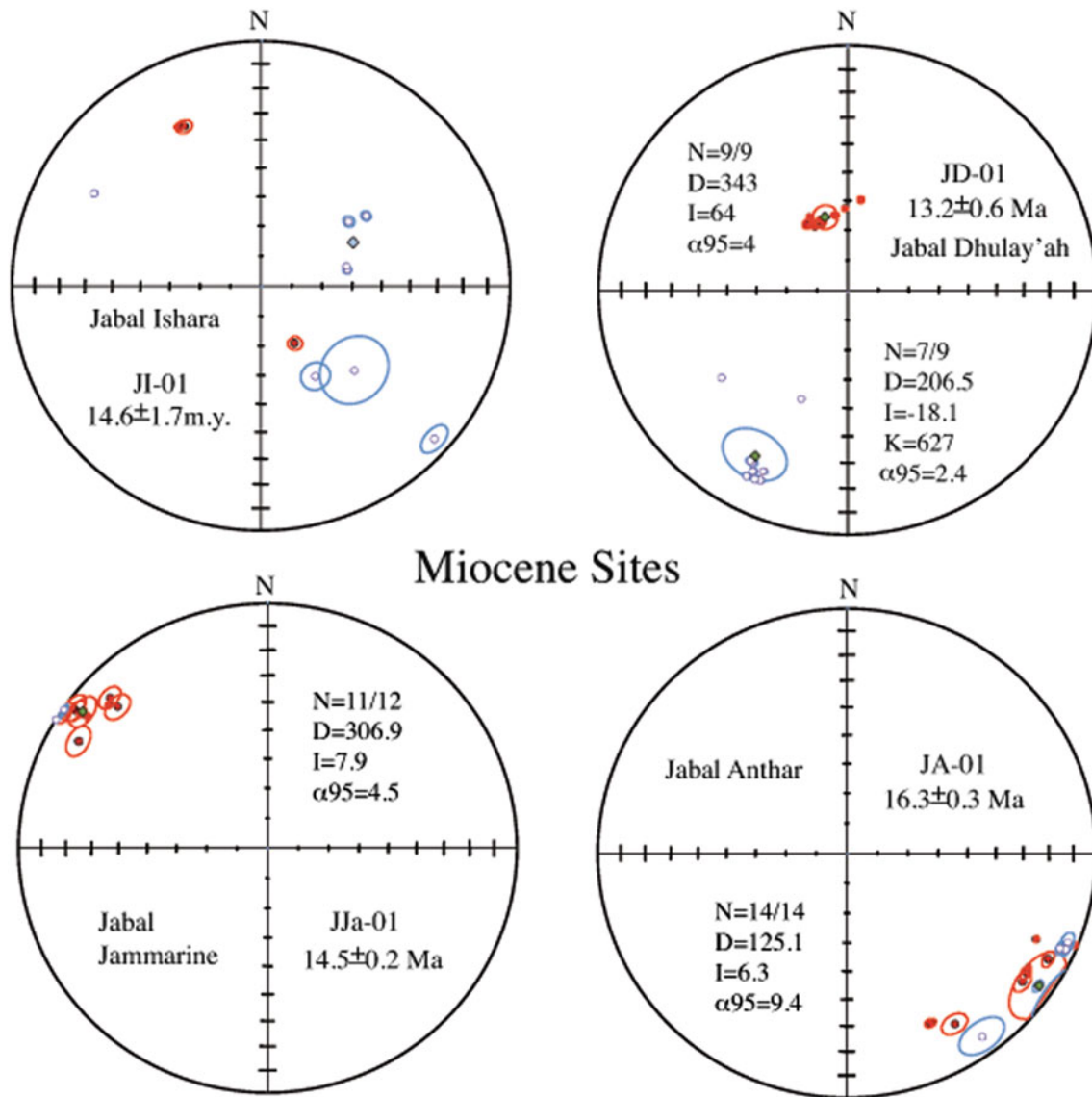


Fig. 7 Equal area projection and mean values of the paleomagnetic data from the Miocene volcanics. Closed (open) symbols refer to positive (negative) inclinations. Open circles represent the MAD of each sample and the α_{95} for the mean value (green square)

implies a paleolatitude (26.4° N) that is in contrast with the northern drift of the Arabian Plate during the Tertiary.

A comparison of the VGP (316.2° E, 80.6° N) with the reference paleopoles from Africa (SAFR; Torsvik et al. 2008) was evaluated using the approach suggested by Demarest (1983). The rotation and flattening values with respect to the Oligocene (30 Ma) paleopole give values that indicate a significant paleomagnetic rotation ($R = 14.86 \pm 6.38^{\circ}$) and differences in latitudes ($F = -10.76 \pm 5.38^{\circ}$). The comparison of the same African pole with the VGP from the As Sarat basaltic flows of Oligocene age (29–24 Ma) studied by Kellogg and Reynolds (1983) point to a smaller counter clockwise rotation (CCW) rotation ($R = -9.65 \pm 4.05^{\circ}$) with a significant and contrasting difference in the flattening ($F = 9.13^{\circ} \pm 4.88^{\circ}$). The

uncertainty in both the age of the rock and magnetization in the Bi'r al' Ayn siltstones could explain the observed differences. Additionally, the As Sarat data show inconsistent antipodal directions that cannot be easily interpreted. The flows with normal ($D = 354.8$; $I = 19$) and reverse polarity ($D = 186.3$; $I = -10.2$) represent two distinct populations that were interpreted by the authors as characteristic of the Earth's magnetic field model described by Wilson (1971). However, as shown by Mc Elhinny (2004), there is no evidence that the normal and reverse mean fields differ from one another. Hence it is more likely that these results reflect partially uncleaned magnetic directions, especially for the lava flows with reverse polarity.

The critical constraint on the timing of the Arabian rotation could be provided by the paleomagnetic data of the Miocene

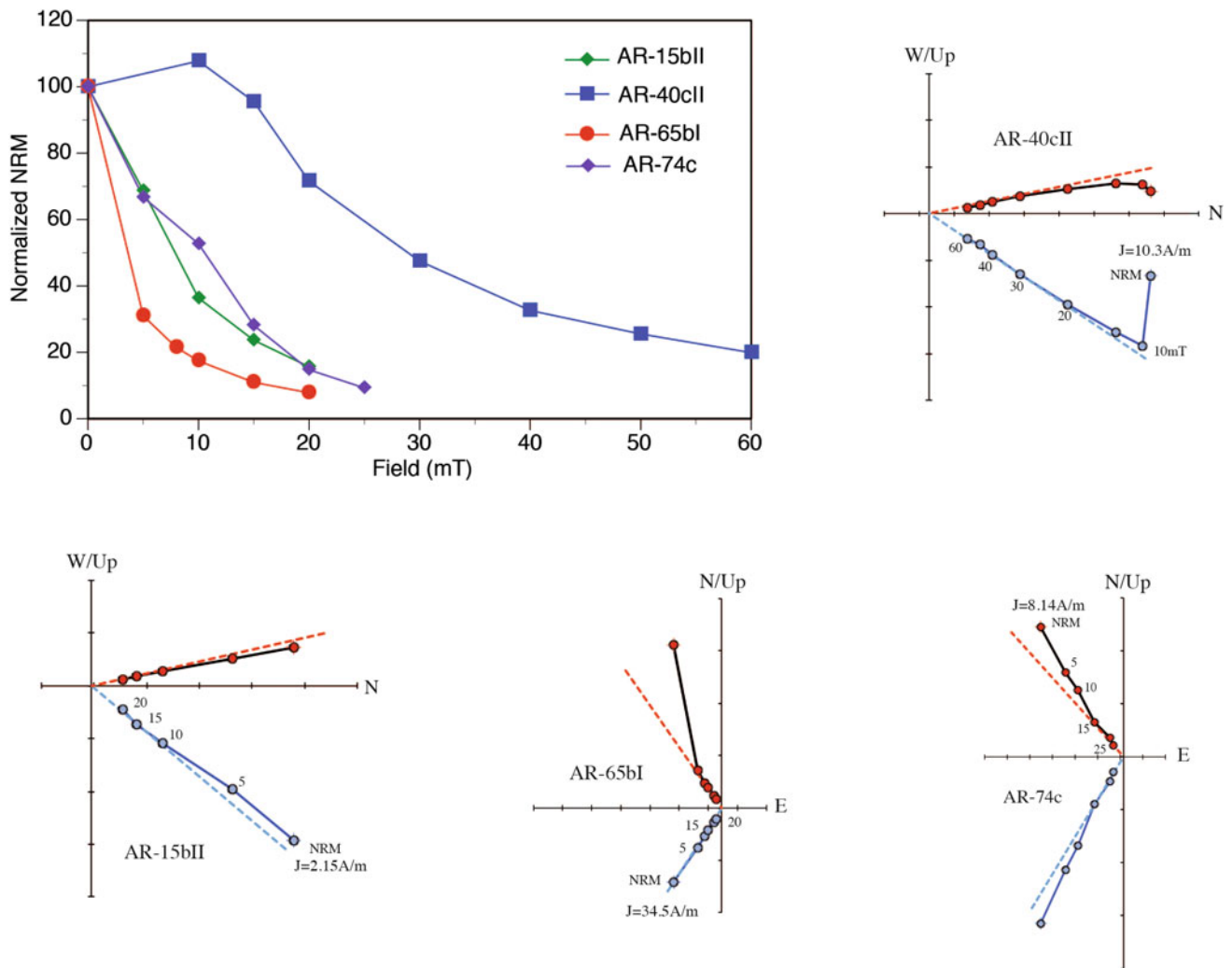


Fig. 8 Normalized intensity of magnetization and orthogonal vector diagrams during AF cleaning of selected samples of Quaternary lava flows from Harrat Lunayyir. Red (blue) circles represent projection onto the horizontal (vertical) plane

rocks and this was the target of our sampling of the Khaybar lava flows. Unfortunately, the quality of the paleomagnetic results from these lava flows is quite poor and certainly inadequate to calculate a mean value representative of a Miocene paleopole for Arabia. The effect of lightning, an artefact that has been observed in several rocks from Arabia (Tarling 1970; Kellog and Reynolds 1983) hampered the possibility of isolating a stable component of magnetization from Jabal Ishara. Meanwhile, contrasting directions from two lava flows collected at Jabal Dhulay'ah could represent only spots of the magnetic field considering that the directions are compatible with secular variations. The results from Jabal Jammazin ($D = 306.9^\circ$; $I = 7.9^\circ$) and Jabal Anthar ($D = 125.1^\circ$; $I = 6.3^\circ$) (Fig. 7) show shallow and almost antipodal directions that are consistently ($57/58^\circ$) CCW deviated with respect to the early Miocene (20 Ma) paleopole for Africa (SAFR; Torsvik et al. 2008). This result cannot be justified by the rotation of the Arabian Plate

since that time. The sub-horizontal bedding of the lava flows excludes tectonic tilt as the main cause for this apparent rotation and additional explanations are necessary. The nature of the outcrops limited the sampling only to the exposed part of the lava flows where the weathering is certainly more pronounced. The low susceptibility and NRM intensity (Fig. 5; Table 2) observed in these rocks is a typical signature of a post-depositional alteration that could be responsible for the anomalous directions. Furthermore, in several outcrops we detected the presence of a strong and deviating local magnetic field caused by the morphology of the cooled parts of the lava. The paleomagnetic record can be significantly affected by this effect if it was already present during the emplacement and cooling of lava flows (Baag et al. 1995; Valet and Soler 1999).

Although some scattering characterizes our late Quaternary volcanics from Lunayyir, the mean value ($D = 0.31^\circ$; $I = 36.9$; $\alpha_{95} = 10.4^\circ$) is indistinguishable from the direction

LUNAYYIR QUATERNARY

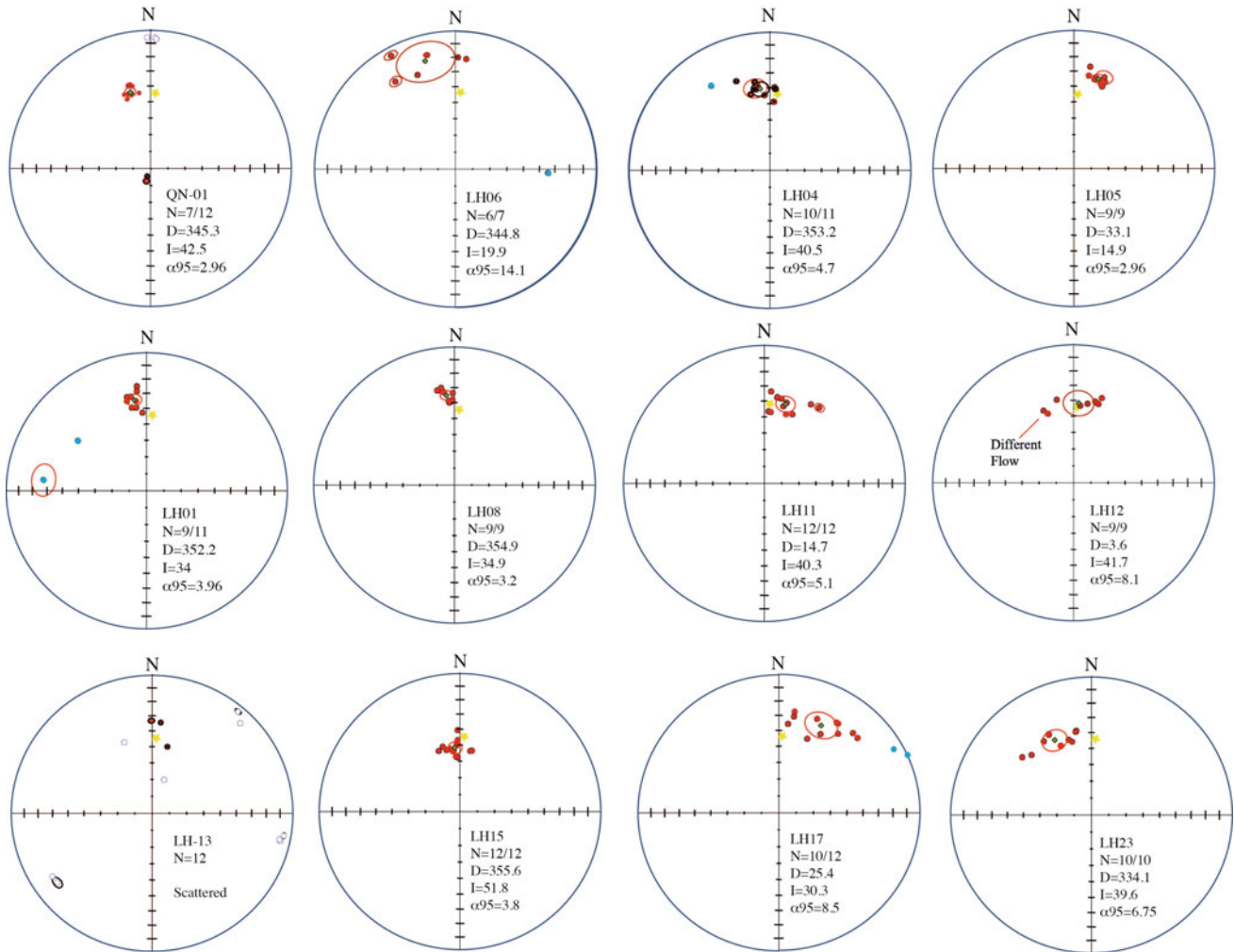


Fig. 9 Equal area projection of the mean paleomagnetic directions and statistical parameter α_{95} for the sites studied in Harrat Lunayyir. Closed (open) symbols refer to positive (negative) inclinations. Symbols in

blue refer to samples excluded by the mean. Open circles represent the MAD of each sample and the α_{95} for the mean value (green square). Yellow star represents the present magnetic field

of the present field, indicating that no rotation occurred since their emplacement. The observed normal polarity suggests that these flows were emplaced during the Brunhes Chron (0–0.78 Ma), in agreement with the ages (<0.57 Ma) reported by Duncan and Al-Amri (2013) for the rocks of Lunayyir. Even though paleomagnetic data have limited use in constraining small rotations, especially if uncertainties are not very small, a comparison with the coeval African paleopole (SAFR; Torsvik et al. 2008) indicates a negligible rotation between the two plates in recent times ($R = -1.98 \pm 10.49^\circ$ and $F = 5.29 \pm 8.68^\circ$).

There are few Tertiary paleomagnetic results from the Arabian Peninsula that can be compared with our data. The middle Pliocene volcanics (age 3.3–3.73 Ma) from Harrat Rahat (Hussain and Bakor 1989) and the early Pliocene volcanics (5 Ma) from Aden (Irving and Tarling 1961)

indicate that about 11° and 7° of CCW rotation occurred since their formation, respectively (Fig. 11a). It should be noted that the amount of rotation of the younger volcanics (middle Pliocene age) is a little bit larger than those of the early Pliocene from Aden, even though statistically they are indistinguishable. These data are in agreement with the Oligocene data from As Sarat (Kellogg and Reynolds 1983) and they seem consistent with our results from the sediments of Bi'r al 'Ayn (Fig. 11a). The existing data seem to indicate that the Arabian Plate undertook a CCW rotation of about 10° with respect to the magnetic pole and about 15° with respect to stable Africa. However, the existing paleomagnetic directions of magnetization and associated pole positions show an agreement from the Oligocene to the Pliocene (Fig. 10), which can be interpreted only by assuming that the entire rotation occurred during the last 4–5 Ma as suggested

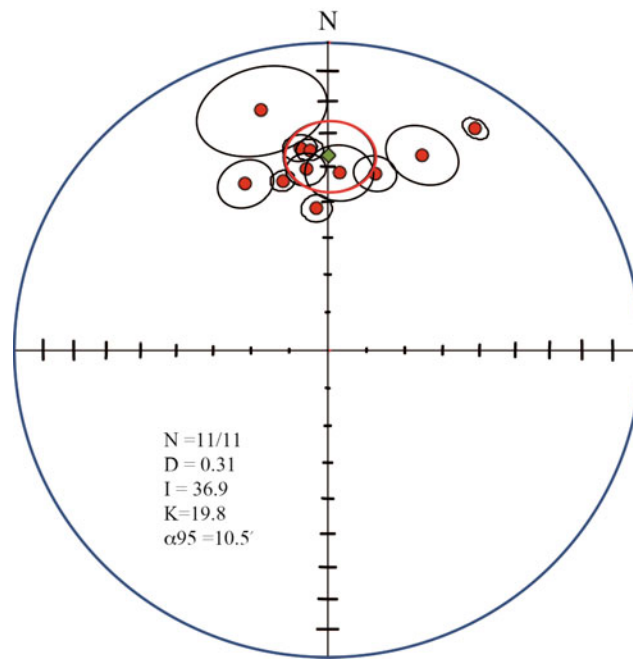
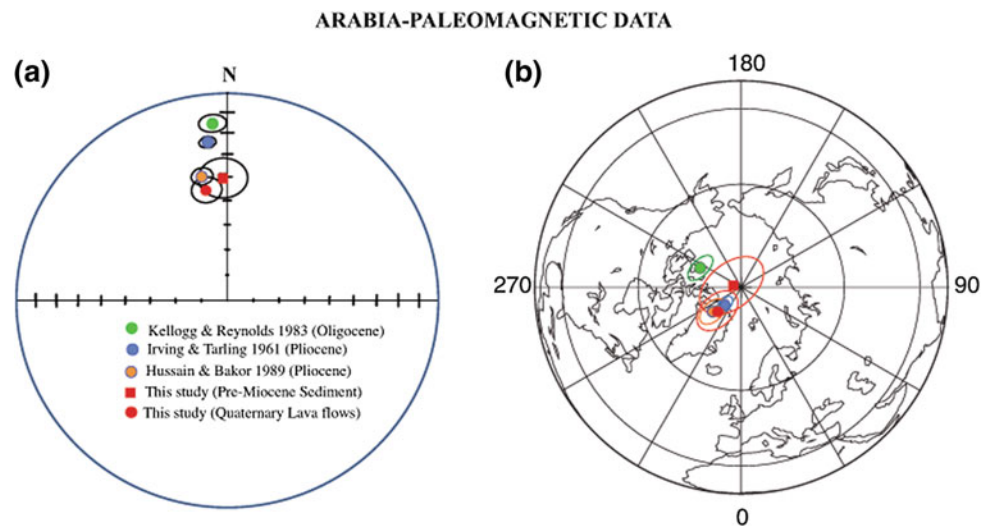


Fig. 10 Equal area projection of the paleomagnetic directions and statistical parameters for the Quaternary volcanics from Harrat Lunayyir. Green square refers to the mean value with α_{95} in red

Fig. 11 Comparison of the paleomagnetic results from this study with the existing paleomagnetic data (a) and relative VGP position (b) for Arabia during the Tertiary. Circles represent uncertainties (α_{95} for the paleomagnetic directions and A_{95} for the poles)



by other authors (Tarling 1970; Kellogg and Reynolds 1983). This would imply that the whole rotation took place during the last phase of the opening that corresponds to true sea-floor spreading. This is in contrast with the hypothesis that suggested different phases of rotation or a constant opening of the Red Sea since the beginning of the rifting (Hall 1979; Girdler 1991; Labreque and Zitellini 1985; Almalki et al. 2015). However, the existing paleomagnetic data are inadequate to enlighten the early rotational history of the Arabian Plate.

The Koenigsberger ratio (Q) (Tables 2 and 3; Fig. 6) is above 1 in all the rocks indicating that the remanence predominates over the induced magnetization and it should be taken into account when interpreting magnetic anomalies. Considering that in the Lunayyir area these data can be integrated with geochemical and petrological data (Duncan and Al-Amri 2013; Sanfilippo et al., this volume) there is a significant data set that could be used to test the reliability of the aeromagnetic data interpretations.

Acknowledgements The research was sponsored by the PRIN2012 Programme (Project 20125JKANY_002) and supported by the Italian Consiglio Nazionale Ricerche and the US National Science Foundation. The authors are grateful to Dr. Aldo Winkler (INGV-Rome) for the measurements of the hysteresis properties and Dr. Marco Ligi for help during the sampling and improvements of the manuscript. This work is the result of a joint effort of the Saudi Geological Survey (SGS) and the Istituto di Scienze Marine, CNR of Bologna (ISMAR-CNR). We particularly thank the SGS team: A.O. Saeedi, A. Zahrani, Z.A. Otaibi, H. H. Subahi, M.M. Khorshid and A.M. Jarees, Captain P. Dimala and helicopter assistants F. Abdulhadi and A. Al-Harbi for their collaboration during the field work. We thank Dr. Z.A. Nawab, SGS President and Dr. A.M. AlAttas, SGS Assistant President for Technical Support.

References

- Almalki KA, Ailleres L, Betts PG, Bantan RA (2015) Evidence for and relationship between recent distributed extension and halokinesis in the Farasan Islands, southern Red Sea, Saudi Arabia. *Arab J Geosci* 8:8753–8766. <https://doi.org/10.1007/s12517-015-1792-9>
- Baag C, Hellsley CE, Xu SZ, Lienert RB (1995) Deflection of paleomagnetic directions due to magnetization of the underlying terrain. *J Geophys Res* 100(B7):10013–10027
- Bayer HJ, El-Isa Z, Hotzl H, Mechie J, Prodehl C, Saffarini G (1989) Large tectonic and lithospheric structures of the Red Sea region. *J African Earth Sci (and the Middle East)* 8(2):565–587. [https://doi.org/10.1016/S0899-5362\(89\)80045-4](https://doi.org/10.1016/S0899-5362(89)80045-4)
- Bosworth W, Stockli DF (2016) Early magmatism in the greater Red Sea rift: timing and significance. *Can J Earth Sci* 53(11):1158–1176. <https://doi.org/10.1139/cjes-2016-0019>
- Brown GF (1970) Eastern margin of the Red Sea and the coastal structures in Saudi Arabia. *Phil Trans Roy Soc London A* 267:75–87
- Burke K, Dewey JF (1973) Plume-generated triple junctions: key indicators in applying plate tectonics to old rocks. *J Geology* 81:406–433
- Camp VE, Roobol MJ (1992) Upwelling asthenosphere beneath western Arabia and its regional implications. *J Geophys Res* 97:15,255–15,271
- Camp VE, Roobol MJ, Hooper PR (1991) The Arabian continental alkali basalt province: part II. Evolution of Harrats Khaybar, Ithnayn, and Kura, Kingdom of Saudi Arabia. *Bull Geol Soc Am* 103:363–391
- Cochran JR (1981) The Gulf of Aden: structure and evolution of a very young ocean basin and continental margin. *J Geophys Res* 86:263–287
- Cogné JP (2003) PaleoMac: a Macintosh™ application for treating paleomagnetic data and making plate reconstructions. *Geochem Geophys Geosyst* 4(1):1007. <https://doi.org/10.1029/2001GC000227>
- Coleman RG, Hadley DG, Fleck RG, Hedge CT, Donato MM (1979) The Miocene Tihama Asir ophiolite and its bearing on the opening of the Red Sea. In: Al-Shanti AM (ed) *Evolution and Mineralization of the Arabian Shield*, vol 1. Pergamon Press, Oxford, pp 173–186
- Coleman RG, Fleck RJ, Hedge CE, Ghent ED (1977) The volcanic rocks of southwest Saudi Arabia and the opening of the Red Sea. *Mineral Resources Bull 22D*, Red Sea Research. Jeddah, Saudi Arabia, pp D1–D30
- Coleman RG, Fleck RJ, Hedge CE, Ghent ED (1975) The volcanic rocks of southwestern Saudi Arabia and the opening of the Red Sea. *U.S. Geol Survey Saudi Arabian Project Report* 194
- Collins WJ (2003) Slab pull, mantle convection, and Pangaean assembly and dispersal. *Earth Planet Sci Lett* 205:225–237. [https://doi.org/10.1016/S0012-821X\(02\)01043-9](https://doi.org/10.1016/S0012-821X(02)01043-9)
- Dalrymple GB, Alexander EC, Lanphere MA, Kraker GP (1981) Irradiation of samples for ⁴⁰Ar/³⁹Ar dating using the Geological Survey TRIGA reactor. In: *USGS Professional Papers*, U.S. Geol Surv, Reston, VA, 1176:29
- Demarest HH (1983) Error analysis for the determination of tectonic rotation from paleomagnetic data. *J Geophys Res* 88:4321–4328. <https://doi.org/10.1029/JB088iB05p04321>
- Dhellemmes R, Delfour J (1979) Geologic map of the Khaybar quadrangle, sheet 25 D, Kingdom of Saudi Arabia (with text). Saudi Arabian Directorate General of Mineral Resources Geologic Map GM-50A, scale 1:250000
- Duncan RA, Al-Amri AM (2013) Timing and composition of volcanic activity at Harrat Lunayyir, western Saudi Arabia. *J Volcanology Geothermal Res* 260:103–116
- Fisher RA (1953) Dispersion on a sphere. *Proc Roy Soc London A* 217:295–305
- Girdler RW, Styles P (1974) Two stage Red Sea floor spreading. *Nature* 247:7–11
- Girdler RW (1983) The evolution of the Gulf of Aden and Red Sea in space and time. In: Angel MY (ed) *Marine science of the northwest Indian Ocean and adjacent waters*. Pergamon Press, New York, p 747
- Girdler RW (1985) Problems concerning the evolution of oceanic lithosphere in the northern Red Sea. *Tectonophysics* 116:109–122
- Girdler RW (1991) The Afro-Arabian rift system—an overview. *Tectonophysics* 197:139–153
- Gradstein FM, Ogg JG, Schmitz M, Ogg G (eds) (2012) *The geologic time scale 2012*. Elsevier, 1144 pp
- Hall SA, Andreassen GE, Girdler RW (1976) Total intensity magnetic anomaly map of the Red Sea and adjacent coastal areas, a description and preliminary interpretation. *U.S. Geol Surv Saudi Arabian Project Rep* 206, 36 pp
- Hall SA (1979) A total intensity magnetic anomaly map of the Red Sea and its interpretation. *U.S. Geol Surv Saudi Arabian Project Rep* 275, 260 pp
- Hussain AG, Bakor AR (1989) Petrography and palaeomagnetism of the basalts, southwest Harrat Rahat, Saudi Arabia. *Geophys J Int* 99:687–698. <https://doi.org/10.1111/j.1365-246x.1989.tb02051.x>
- Irving E, Tarling DH (1961) The palaeomagnetism of the Aden volcanics. *J Geophys Res* 66:549–555
- Johnson RW, Knutson J, Taylor SR (eds) (1989) *Intraplate volcanism in eastern Australia and New Zealand*. Cambridge University Press, Cambridge, UK, p 408
- Jones PW, Rex DC (1974) New dates from the Ethiopian plateau volcanic. *Nature* 252:218–219
- Kellogg KS, Reynolds RC (1983) Opening of the Red Sea: constraints from a paleomagnetic study of the As Sarat volcanic field, south-western Saudi Arabia. *Geophys J R Astron Soc* 74:649–665
- Kemp J (1981) Explanatory notes to the geological map of the Wadi al' Ays quadrangle, sheet 25C, Kingdom of Saudi Arabia. Ministry of Petroleum and Mineral Resources, Saudi Arabia, 39 pp
- Kirschvink JL (1980) The least-squares line and plane and the analysis of palaeomagnetic data. *Geophys J Int* 62:699–718
- Kuiper KF, Deino A, Hilgen FJ, Krijgsman W, Renne PR, Wijbrans JR (2008) Synchronizing rock clocks of Earth history. *Science* 320:500–504. <https://doi.org/10.1126/science.1154339>
- Labrecque JL, Zitellini N (1985) Continuous seafloor spreading in Red Sea: an alternative interpretation of magnetic anomaly pattern. *Bull Am Assoc Pet Geol* 69:513–524
- Le Pichon X, Franchetcau J (1978) A plate tectonic analysis of the Red Sea-Gulf of Aden area. *Tectonophysics* 46:369–406

- McElhinny M (2004) Geocentric axial dipole hypothesis: a least squares perspective. In: Channell JET, Kent DV, Lowrie W, Meert JG (eds) Timescales of the paleomagnetic field. Am Geophys Union, Washington, DC. <https://doi.org/10.1029/145gm01>
- McKenzie D, Davies D, Molnar P (1970) Plate tectonics of the Red Sea and East Africa. *Nature* 226:243–248
- Pellaton C, Dhellemes R (1978) Geology and mineral exploration of the Jabal Dhulay'ah quadrangle, 25/38A. Bureau de Recherches Geologiques et Minières Technical Record 78-JED-3, 16 p, 1 fig., 2 maps, 1 app
- Reilinger R, McClusky S, Ar Rajehi A (2015) Geodetic constraints on the geodynamic evolution of the Red Sea. In: Rasul NMA, Stewart ICF (eds) The Red Sea: the formation, morphology, oceanography and environment of a young ocean basin. Springer Earth System Sciences, Berlin Heidelberg, pp 135–149
- Roeser HA (1975) A detailed magnetic survey of the southern Red Sea. *Geol Jahrb* 13:131–153
- Sagnotti L (2013) Demagnetization analysis in Excel (DAIE)—An open source workbook in Excel for viewing and analyzing demagnetization data from paleomagnetic discrete samples and u-channels. *Annals Geophys* 56(1):D0114. <https://doi.org/10.4401/ag-6282>
- Sanfilippo A, Cai Y, Gouveia Jácome AP, Ligi M (this volume) Geochemistry of the Lunayyir and Khaybar volcanic fields (Saudi Arabia): Insights into the origin of Cenozoic Arabian volcanism
- Schettino A, Macchiavelli C, Rasul N (this volume) Plate motions around the Red Sea since the Early Oligocene
- Stern RJ, Johnson PR (this volume) Constraining the opening of the Red Sea: evidence from the Neoproterozoic margins and Cenozoic magmatism for a Volcanic Rifted Margin
- Tarling DH (1970) Palaeomagnetism and the origin of the Red Sea and the Gulf of Aden. *Phil Trans Roy Soc A* 267:219–226
- Tapponnier P, Francheteau J (1978) Necking of the lithosphere and the mechanics of slowly accreting plate boundaries. *J Geophys Res* 83:3955–3970. <https://doi.org/10.1029/JB083iB08p03955>
- Torsvik TH, Müller RD, Van der Voo R, Steinberger B, Gaina C (2008) Global plate motion frames: toward a unified model. *Rev Geophys* 46:RG3004. <https://doi.org/10.1029/2007rg000227>
- Valet JP, Soler V (1999) Magnetic anomalies of lava fields in the Canary Islands: possible consequences for paleomagnetic records. *Phys Earth Planet Int* 115:109–118
- Wegener A (1929) *Die Entstehung der Kontinente und Ozeane*, 4th edn. Friedrich Vieweg and Sohn, Braunschweig
- Wilson RL (1971) Dipole offset—the time average palaeomagnetic field over the past 25 million years. *Geophys J R Astr Soc* 22:491–504